J Mater Sci

Energy materials

Electrochemical analysis of nanoporous carbons derived from activation of polypyrrole for stable supercapacitors

Belinda Moyo[1], Damilola Momodu[1], Oladepo Fasakin[1,2], Abdulhakeem Bello[1,3], Julien Dangbegnon[1], and Ncholu Manyala[1,*]

[1] *Department of Physics, Institute of Applied Materials, SARCHI Chair in Carbon Technology and Materials, University of Pretoria, Pretoria 0028, South Africa*

[2] *Department of Physics, Obafemi Awolowo University, Ile-Ife 220005, Nigeria*

[3] *Department of Materials Science and Engineering, African University of Science and Technology (AUST), Abuja, Federal Capital Territory, Nigeria*

Received: 24 October 2017
Accepted: 8 December 2017

ABSTRACT

In this study, activated carbon was derived from polypyrrole (PPY) using a K_2CO_3 activating agent with varying mass ratios of the activating agent to PPY polymer (AA:PP), for the optimization of the hierarchical pore structure necessary for improved electrochemical performance. The textural study of the as-synthesized samples (AC-PPY) displayed an increase in the specific surface area (SSA) and pore volume with increase in the amount of the activating agent up to a threshold for AA:PP of 6:1. The increase in the SSA was due to the presence of hierarchical pores in the material structure for efficient ion penetration. Initial half-cell electrochemical tests performed on the different activated carbon samples with varying SSA revealed superior charge storage capability for the 6:1 sample in both negative and positive operating potentials. The highest current response value was obtained from the signatory EDLC-type cyclic voltammogram, along with the longest discharge time from the chronopotentiometry plot as a result of the lowest ion diffusion length for successful fast ion transport reported from the impedance spectroscopy analysis. A full symmetric device (AC-PPY-6) assembled from the best material using KNO_3 neutral electrolyte yielded a specific capacitance of 140 F g^{-1}, 12.4 Wh kg^{-1} energy density at 0.5 A g^{-1} gravimetric current. An energy density of 7.12 Wh kg^{-1} was still maintained at a specific current of 2 A g^{-1}. Interestingly, after the ageing test to ascertain device stability, the device energy density increased back to 12.2 Wh kg^{-1} as a result of the creation of additional active pores within the nanostructured material for charge storage via voltage holding tests which also led to the enhancement in specific capacitance to 137.5 F g^{-1} at 2 A g^{-1}. A 99.0% capacitance retention was recorded even after 10000 cycles at a moderate

Address correspondence to E-mail: ncholu.manyala@up.ac.za

https://doi.org/10.1007/s10853-017-1911-y

Published online: 18 December 2017

specific current of 2 A g^{-1}. A substantial approach was used to elucidate the degradation phenomena from the device self-discharge profile, which showcased the device retaining up to 70% of its operating potential after 80 h (> 3 days) on open circuit. The results obtained demonstrate the potential of adopting the AC-PPY material in potential device for energy storage purposes.

Introduction

The exponentially increasing global demand for energy, coupled with the fossil fuels consumption and the related greenhouse gas (CO_2) emissions causing global warming [1], has led to the search for alternative energy sources. This has also led to the development of new technologies using renewable, clean and sustainable energy resources over the last couple of decades. However, one of the major issues underplaying these new technologies lies in the ability to store and supply the generated energy based on specific requirements in addition to the generated surplus in some instances which might not be needed at that occasion. Efficient energy storage technologies, such as batteries and recently supercapacitors, have been at the forefront of this research and are essentially exploited to proffer solution to the current energy crisis.

Supercapacitors (SCs) are high power technological devices capable of powering portable electronic devices and transportation systems due to their quick power delivery and extended cycle life [2, 3]. The charging time of SCs ranges from seconds to minutes which brings about their fast energy harvesting, but SCs store less energy when compared with most batteries [4]. Nevertheless, efforts to improve the SCs performance without sacrificing their high power density and cycling life need to be further explored, especially through exploring cheaper and new classes of electrode materials, (including oxides, 2-D materials, sulphides, transition metal carbides) and also the electrolytes [4]. Carbon is the typical material adopted in electrochemical double-layer capacitors (EDLCs) in which the charge storage occurs at the electrode–electrolyte interface. In particular, activated carbons (ACs) are the only commercially available carbon used in the energy storage industry due to its adequate porosity, high specific surface area, high electrical conductivity and good chemical stability [5–7].

Many of the ACs produced are based on template methods and are very efficient for the production of porous carbon with excellent and tuneable properties [8–10]. However, the difficulty with template-based approach is the usage of expensive materials such as silica and zeolite as templates [11, 12]. Other techniques adopted for the production of the carbon materials are the chemical and physical methods [13, 14]. The chemical treatment usually results in the formation of an aerogel or hydrogel material while the physical method (activation mostly with KOH, $ZnCl_2$ and H_3PO_4) and carbonization at elevated temperatures lead to the formation of porous carbons [15–17].

Many research groups have adopted the latter approach for the production of porous carbon from diverse sources of carbon ranging from inorganic to organic and biomass sources. For example, hydrochars were transformed into porous carbons via hydrothermal carbonization by Wei et al. [18]. Three-dimensional hierarchical porous carbon using KOH activation was reported for use in high-performance supercapacitors by Qie et al. [19]. The as-obtained carbon displayed a large specific surface area (SSA) of about 2870 $m^2\ g^{-1}$, high-level of heteroatom doping (N: 7.7 wt%, O: 12.4 wt%) and good electrical conductivity (5.6 S cm^{-1}). Furthermore, ultrahigh surface area carbon based on polypyrrole was obtained via chemical activation of polypyrrole with KOH by Sevilla et al. [20]. The as-synthesized carbon exhibited an excellent gravimetric and volumetric capacity due to the fact that their high porosity ensured high packing density. Pinecone biomass was also converted into porous carbon via KOH activation and carbonization at 800 °C. The porous carbon material exhibited a mesoporous framework with a SSA of 1515 $m^2\ g^{-1}$, a gravimetric capacitance of 137 F g^{-1}, energy density of 19 Wh kg^{-1} in 1 M Na_2SO_4 electrolyte within a 2.0 V operating voltage [21]. In similar processes related to KOH activation, porous carbons derived from tree bark biomass were also explored as possible electrodes for electrochemical application with an optimization of the synthesis conditions [22].

Very recently, a new perspective has evolved in the materials activation field to produce porous carbons with less negative impact on the environment. This is due to the fact that KOH activation which is the common activating route is perceived to have environmental issues due to corrosive effects (highly alkaline) of KOH, which limits its use on a large scale [23]. Thus, environmentally benign approaches to produce porous carbons are necessary. Recently, a green approach towards achieving microporous carbon materials for high-performance supercapacitor electrodes was reported [23]. The activation of the materials was carried out via a mild chemical activation of the samples with potassium bicarbonate ($KHCO_3$), where it was concluded that the environmental benefits of this activating agent are supplemented by a 10% increase in the yield. It was also reported that the morphology of the starting material is retained after activation, ensuring better packing properties along with a reduced ion diffusion distances, all beneficial for improved electrochemical performance. Based on this, the motivation was developed to explore a similar activating agent potassium carbonate (K_2CO_3) to produce porous carbon from a conducting polymer known as polypyrrole (PPY). Our choice of the activating agent originally lies in the above-mentioned characteristics owing to the fact that $KHCO_3$ still decomposes to form K_2CO_3 which also retains the material morphology as reported earlier. PPY in its capacity also has a higher density and conductivity when compared to other conducting polymers [24], which we believe will lead to porous carbon materials with good electronic properties. PPY is a cost-effective and environmentally stable polymer with high conductivity and can provide high electrochemical performance in small volumes, and it is highly flexible [25–27]. Studies have recently been conducted to look into the flexible nature of PPY and its influence as a supercapacitor. According to Huang et al. [26], the intrinsic stretching ability of the material can maintain or enhance its performance.

Thus, in this work, we present the electrochemical performance analysis of a PPY-derived nanoporous carbon material electrode in a neutral 2.5 M KNO_3 aqueous electrolyte. Most importantly, the device fabricated was relatively stable at a high voltage of 1.6 V, exhibiting an energy density of 12.4 Wh kg^{-1}, excellent capacitance retention of 99% (only a 1% loss) for up to 10000 cycles, which was improved through floating test. The self-discharge test performed also showcased the material retaining up to 70% of its operating voltage for up to 80 h. The results obtained from this study further provide more information into efficiently designing supercapacitor devices for efficient use in energy storage units.

Experimental

Synthesis of activated carbon of polypyrrole

Polypyrrole (PPY) was prepared via a procedure reported previously [28]. The obtained PPY powder was mixed chemically with potassium carbonate anhydrous (K_2CO_3) in different K_2CO_3 mass proportions denoted as 0:1, 2:1, 4:1, 6:1 and 8:1, respectively. Each sample was then carbonized for 2 h at 800 °C with a ramping rate of 5 °C/min under argon gas flow. The activated carbon was then sonicated in 1 M HCl to remove the remaining unreacted salts and continuously rinsed with de-ionized water to attain a neutral pH. Oven drying was done at 60 °C for 12 h.

Physico-chemical characterization

The material textural properties were obtained using the Brunauer–Emmett–Teller (BET) technique from a Micrometrics Tristar II 3020 (version 2.00) Analyser at − 196 °C. The pore size distribution plot was obtained from the desorption branch of the Barrett–Joyner–Halenda (BJH) plots.

Scanning electron microscopy technique (using a Zeiss Ultra plus field emission scanning electron microscope, FESEM) was used to study the morphological properties of the as-synthesized activated carbon from polypyrrole denoted as AC-PPY-X henceforth, with $X = 0$, 2, 4, 6 and 8 for K_2CO_3:PPY ratio of 0:1, 2:1, 4:1, 6:1 and 8:1, respectively. The elements present in the prepared activated carbon were also revealed using energy dispersive X-ray (EDX) analyser attached to the FESEM. The EDX sample was prepared by mixing epoxy resin with the active material and allowed to solidify in an electric oven at 60 °C for 36 h.

The Raman spectra for the samples were obtained using a micro-Raman WITec confocal system preset to a 532-nm-wavelength laser at 50 mW power. The images were focused using a 50× objective lens, which was used to optimize the Raman spectra response.

Electrochemical characterization

Electrochemical analysis of the AC-PPY-X samples was done on a VMP300 Bio-Logic instrument. The electrodes were prepared by mixing the active AC-PPY-X material with polyvinylidene fluoride (PVDF) binder, carbon black in a mass ratio of 80:10:10 and few drops *N*-methyl-2-pyrrolidone (NMP) to make slurry. The slurry was homogeneously coated on nickel foam (NF) current collector and dried at 60 °C. Three-electrode measurements were taken initially to fully understand the charge storage behaviour of the half-cell electrode in a 2.5 M KNO_3 electrolyte using an Ag/AgCl reference electrode and glassy carbon counter electrode.

A symmetric electrochemical capacitor device was subsequently assembled in a coin cell type configuration with filter paper as the separator and 2.5 M KNO_3 as the operating electrolyte. The total mass of active material per unit area on each electrode in the full device was ca. 2.30 mg cm^{-2}. The cyclic voltammetry (CV) and chronopotentiometry (CP) measurements were investigated at different scan rates and gravimetric current densities, respectively. The electrochemical impedance spectroscopy (EIS) tests were run in a frequency range of 100 kHz to 0.01 Hz at open circuit potential. The specific capacitance of a single electrode was calculated from the slope of the CP plot according to Eqs. (1) and (2):

$$C_{\mathrm{el}} = \frac{4I\Delta_t}{\Delta V_{\mathrm{m}}} \tag{1}$$

$$C_{\mathrm{sp}} = \frac{C_{\mathrm{el}}}{4} \tag{2}$$

The energy density and the corresponding power density of the complete device were calculated according to Eqs. (3) and (4):

$$E_{\mathrm{d}} = \frac{1}{2}C_{\mathrm{sp}}(\Delta V)^2 = \frac{C_{\mathrm{el}}(\Delta V)^2}{28.8}\ (\mathrm{Wh\,kg^{-1}}), \tag{3}$$

$$P_{\mathrm{d}} = 3600\frac{E_{\mathrm{d}}}{\Delta t}(\mathrm{W\,kg^{-1}}), \tag{4}$$

where m is the total mass of the electrode material, C_{el} is the specific capacitance of a single electrode, C_{sp} is the specific capacitance of the cell, I is the current applied, Δt is the discharge duration and ΔV is the device voltage window.

Results

The results from the textural analysis done on the as-synthesized AC-PPY samples (shown in Fig. 1) displayed the N_2-absorption–desorption isotherm of type VI with a hysteresis loop present, which is attributed to the adsorbate condensation in the hierarchical pores within the porous carbon materials [29]. The quantity of gas absorbed was observed to increase as the amount of K_2CO_3 was added to the raw material up to a limiting point "*X*" at 6:1 (AA:PP) after which it decreased. This observation is suggested to be due to pore enlargement and possible breakdown of the porous carbon framework by excess activating agent leading to the widening and possible collapse of pore sites [22, 30]. Figure 1b shows the associated plot illustrating the exact values of BET SSA variance with activating agent ratio. As observed, a drop is observed once the ratio exceeded 6.

The pore size distribution (PSD) plot (Fig. 1c) calculated by the Barrett–Joyner–Halenda (BJH) branch shows the nature of the pore range present within the activated carbon sample.

A combination of micropores and mesopores is observed from the PSD plot. A summary of the BET SSA and pore sizes for the AA:PPY-X samples is tabulated in Table 1.

The structural characteristic of the carbon material was investigated using the observed peaks obtained from the Raman spectroscopy tests. Figure 1d displays the Raman spectra for the pristine AC-PPY material without any activating agent as well as those for the activated carbon samples with varying activating agent content. A distinct peak (*) is recorded at a wavenumber of 1100 cm^{-1}, which is linked to the pristine polymer material due to the fact that this peak is present in all activated samples.

However, the intensity of the peak reduces with the introduction of an activation/carbonization process.

This is likely due to the conversion of the polymer into disordered graphitic carbon. For all other samples activated and carbonized, the distinct D- and G-peaks are obtained which confirms the successful conversion of the polymer into a highly disordered carbonaceous material [31].

This agrees with results [32, 33] obtained from other studies with similar porous activated carbon material and thus confirms the presence of sp^2 graphitic-type carbon with C–C bonds.

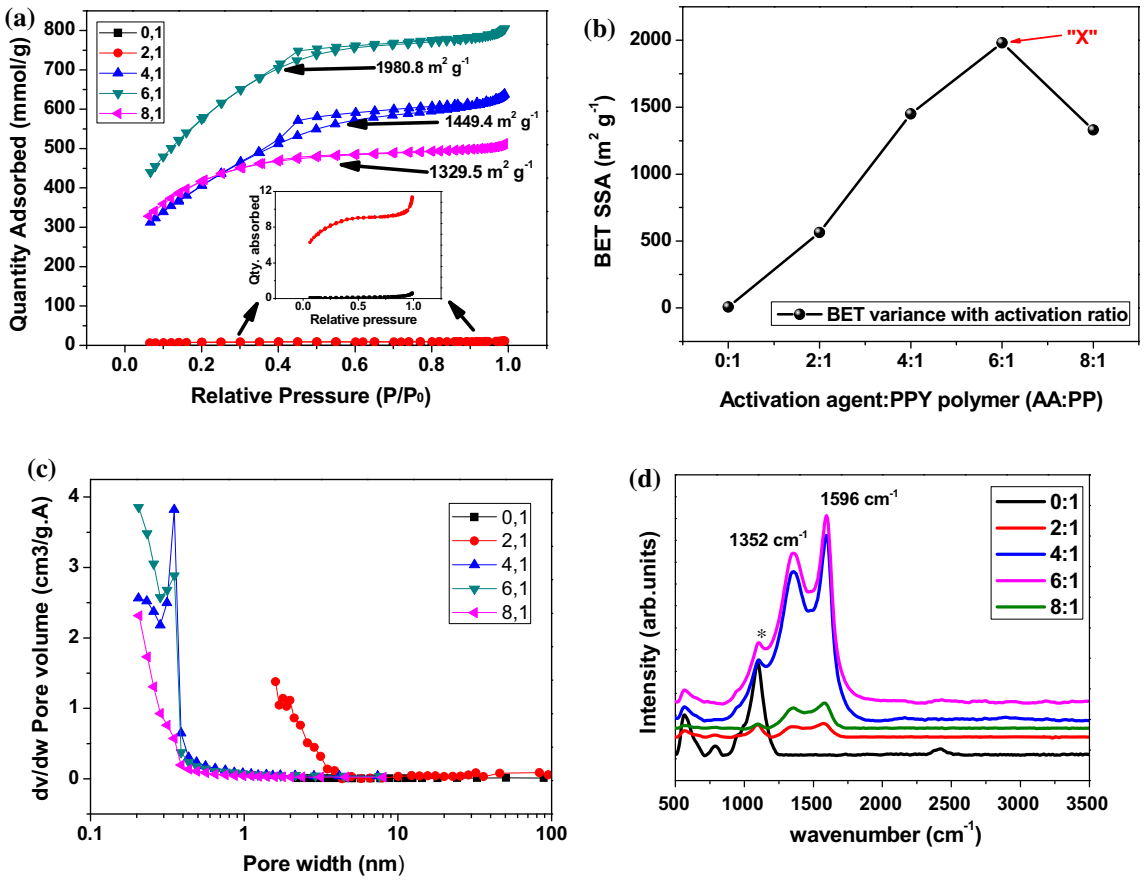

Figure 1 **a** N_2 absorption/desorption isotherm, **b** variance of BET SSA with activating agent content, **c** pore size distribution plots for the different activated samples from PPY-conductive polymer and **d** Raman spectra of the different activated samples showing the distinct carbonaceous D- and G-peaks.

Table 1 Summary of textural properties of activated carbon from PPY samples

Sample	Specific surface area (S_{BET}, $m^2\ g^{-1}$)	Total pore volume (V, $cm^3\ g^{-1}$)	Micropore volume (V_{micro}, $cm^3\ g^{-1}$)	Mesopore volume (V_{meso}, $cm^3\ g^{-1}$)	Average pore diameter (nm)
0:1	7.57	0.02	0.00	0.02	9.82
2:1	562.83	0.38	0.057	0.32	2.68
4:1	1449.42	0.98	0.019	0.96	2.75
6:1	1980.81	1.24	0.029	1.21	2.50
8:1	1329.47	0.79	0.14	0.65	2.38

To endorse the potential use of this material for supercapacitor application, the electrochemical performance of the AC-PPY electrode material was evaluated in a three-electrode system with 2.5 M KNO_3 as the aqueous electrolyte.

Firstly, cyclic voltammetry (CV) and chronopotentiometry (or galvanostatic charge–discharge) (CP or GCD) measurements were taken. Figure 2a shows the CV curves of all electrode materials activated with different K_2CO_3:PPY ratio at 20 mV s^{-1}. The samples all exhibited rectangular-shaped CV curves between 0 and 0.8 V, showing the typical EDLC behaviour. Furthermore, the charge separation (current response) seems to be enhanced with increasing K_2CO_3:PPY ratio up to 6:1 before diminishing with higher K_2CO_3:PPY ratio. The electrochemical performance is found to be intimately related to the K_2CO_3:PPY used during the electrode material preparation as shown from the BET SSA in Fig. 1b. Explicitly, both the BET SSA and charge separation

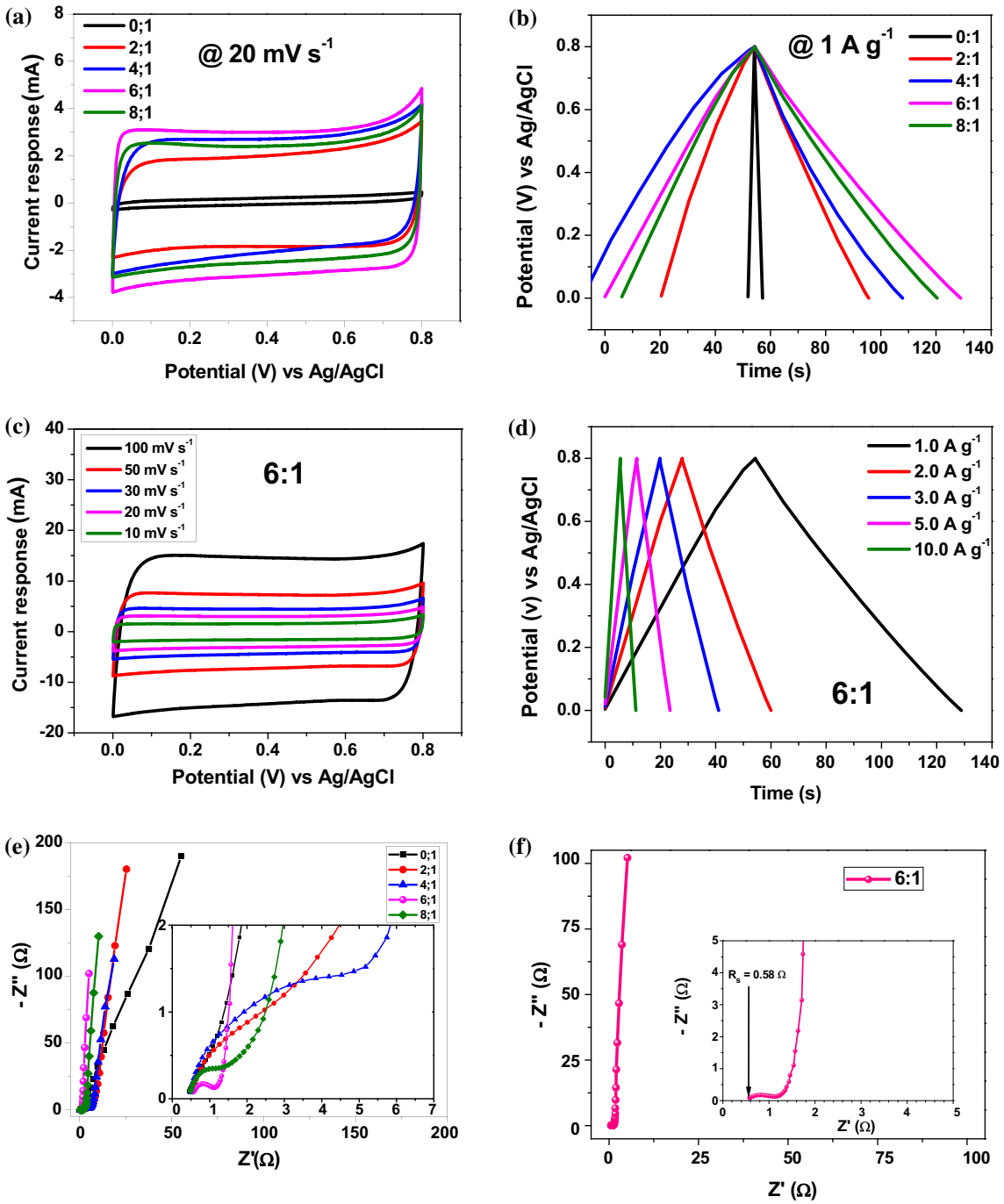

Figure 2 **a**, **b** Cyclic voltammetry (CV) and associated chronopotentiometry (CP) plots of activated carbon from PPY (AC-PPY) with varying quantities of K_2CO_3; **c**, **d** detailed CV and the related CP profile of AC-PPY-6 sample at varying scan rates and current densities; **e**, **f** EIS plot of the AC-PPY-X electrodes for different quantities of K_2CO3 and **f** the AC-PPY-6 sample in a 2.5 M KNO_3 electrolyte.

increase with increasing K_2CO_3:PPY ratio, reaching a maximum value at a ratio of 6:1. Upon introduction of more activating agent, a decrease in current response was recorded showing that the best sample is the one synthesized at a ratio of 6:1.

For this ratio, the higher SSA and the presence of hierarchical micropores necessary for storage and high power performance at high gravimetric current will boost its capacitive performance. Furthermore, the observed rectangular shape of the CV profile

suggests small resistive behaviour for this electrode material.

Figure 2b shows the CD plots of all electrode materials at a current density of 1 A g^{-1}. Typical triangular-shaped CD curves for EDLCs are observed for all electrodes. In addition, the discharge time and consequently the capacitance increase with increasing K_2CO_3:PPY ratio up to 6:1. Additional increase in the ratio led to a decreased discharge time and charge storage capacity. It is observed that the 4:1 sample had a longer charge period as compared to discharge process. It is suggested that this is due to the presence of functional groups which are only active during the charging step but become inactive during the discharge process.

This is in good agreement with the CV results, confirming the high capacitive performance of the electrode synthesized with a K_2CO_3:PPY ratio of 6:1. The best electrode was further analysed by varying the sweep rate and the current density. Figure 2c shows the CV curves of AC-PPY-6 at different current densities. The rectangular shape is preserved even at a high scan rate of 100 mV s^{-1}, with no apparent distortion when compared to its shape at lower sweep rate. This confirms the insignificant resistive behaviour of the electrode material, which could otherwise reduce the capacitive performance of the electrode material.

Figure 2d displays the CP plot of the AC-PPY-6 electrode at different values of gravimetric current. The triangular curve is visible for all current densities with no significant IR drop, confirming the low equivalent internal resistance of the electrode.

To fully understand the electrical properties and electrochemical performance of the carbon-based electrode materials, EIS measurements were also taken and the results are shown in Fig. 2e.

The solution resistance which is equivalent to the equivalent series resistance (ESR) is approx. 0.5 Ω for all electrodes. However, the discrepancy appears for the charge transfer resistance (R_{ct}) obtained from the diameter of the semicircular part of the Nyquist plot in the high-frequency region. The electrode material activated with K_2CO_3:PPY in ratio of 6:1 displayed the smallest R_{ct} value with the shortest diffusion length.

The angle of the Nyquist plot with the Z'-axis at the low-frequency region defines the capacitive behaviour of the material electrode [34]. An ideal capacitor has a complete vertical line which is parallel to the imaginary impedance axis at the low-frequency region. The AC-PPY-6 sample displays the capacitive response closest to the ideal capacitance. The results from the impedance spectroscopy analysis are in good agreement with the results discussed in Fig. 2a.

In summary, the AC-PPY-6 material has the lowest leakage current associated with the highest charge separation, longest discharge time and highest BET SSA, as compared to the other electrode materials with varying K_2CO_3 content. Therefore, activation of the PPY with K_2CO_3 in a AA:PP ratio of 6:1 gives a material with the best electrochemical performance necessary for energy storage application.

The AC-PPY-6 nanostructured material electrode was further used in the fabrication of a full symmetric device. As shown in Fig. S2(a), this electrode works symmetrically from − 0.8 to 0 V and from 0 to 0.8 V, with very similar current response. This predicts a stable working potential window of 1.6 V for the full cell, as shown in Fig. 3a, which displays the CV profile of the full cell at different scan rates.

The rectangular shape is still maintained for scan rate up to 50 mV s^{-1}, demonstrating the fast ion diffusion kinetics and the fast current response on voltage reversal of this electrode.

Figure 3b shows the CP plot of the symmetric supercapacitor at different current densities. The triangular shape remains for all the applied current density values, exhibiting a good capacitive behaviour. The specific capacitance calculated from the CP plots is displayed in Fig. 3c.

The specific capacitance showed a steep decrease from 140 to 80 F g^{-1} when the current density was increased from 0.5 to 2.0 A g^{-1}. In other words, more than half of the initial capacitance is retained when the current density is quadrupled. Further increase in the current density has less significant effect on the specific capacitance which varied from 80 to 65 F g^{-1} for an increase in current density from 2.0 to 10.0 A g^{-1}. This corresponds to an impressive 81% of capacitance retention between 2.0 and 10.0 A g^{-1}.

This high rate capability is not only related to the fast diffusion kinetic of the electrolyte ions but also to the existence of suitable pores contained within the active electrode material required for energy storage application. Figure 3d shows the Ragone plot of the symmetric cell.

A high energy density of 12.4 Wh kg^{-1} corresponding to a power density of 415 W kg^{-1} is calculated at a

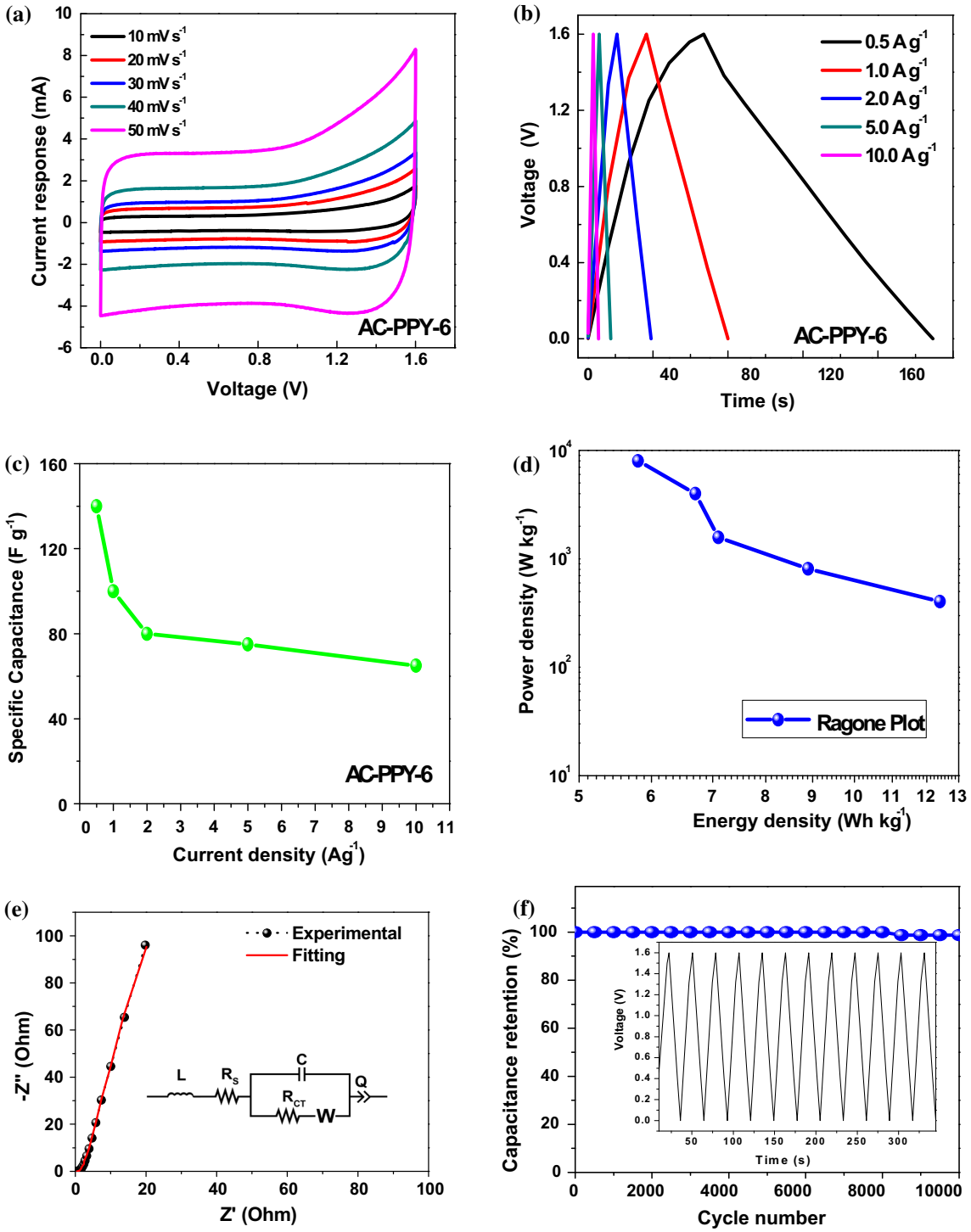

Figure 3 Electrochemical performances of the AC-PPY-6 symmetric device showing **a**, **b** CV and CP plots at different scan rates and gravimetric current densities; **c** associated specific capacitance as a function of gravimetric current density; **d** relationship between energy density and power density; **e** EIS plot showing the equivalent series circuit fitted to the plot and **f** capacitance retention versus cycle number with the figure inset showing a few galvanostatic charge–discharge cycles at 2 A g^{-1}.

current density of 0.5 A g^{-1}. The energy density remained at 5.8 Wh kg^{-1} corresponding to a power density of 8 kW kg^{-1} at a current density of 10 A g^{-1}.

The cycling stability of the cell was also investigated with continuous charging–discharging for up to 10000 cycles at a current density of 2 A g^{-1} (see Fig. 3f).

The cell retained 99% of its initial capacitance up to 10000 cycles, hinting at a negligible deterioration of the electrode material upon cycling.

Figure S2(b) shows the EIS Nyquist plot before and after cycling. An increase in the R_s value as well as the decrease in the ideal EDLC response based on the slope of the Nyquist plot in the low-frequency region was observed after cycling, which accounts for the slight decrease in specific capacitance.

Further ageing test was done by alternately holding the cell at its maximum voltage for an extended period of time while subjecting the device to constant charging–discharging steps at every 10 h intervals for more than 3 days. The specific capacitance was calculated from the average discharge time from the charge–discharge plot at each 10 h interval, and the result is presented in Fig. 4a. This experiment aimed at studying any deteriorating effect from holding the device at its maximum operating voltage for a prolonged period of time.

The result obtained can be divided into four steps: an increase in specific capacitance after the first 10 h of voltage holding, a constant device specific capacitance recorded from 10 to 40 h, a further increase in the specific capacitance from 40 to 60 h before stabilizing onwards. The first increase could be related to the time needed for a good wettability of the electrolyte on the surface of the electrode material. In other terms, within the first 10 h, the wettability of the electrode material could improve and subsequently more ions are stored at the electrode/electrolyte interface. The second increase is most likely related to the availability of more pores which were not participating in the initial storage process. The accessibility of these new pores is due to the repeated cycling and voltage holding, which could force the ions into these hidden pores. It is worth noting that the specific capacitance has almost doubled after the ageing experiment, increasing from 75 to 137.5 F g^{-1}. This will also result in an increase in the energy

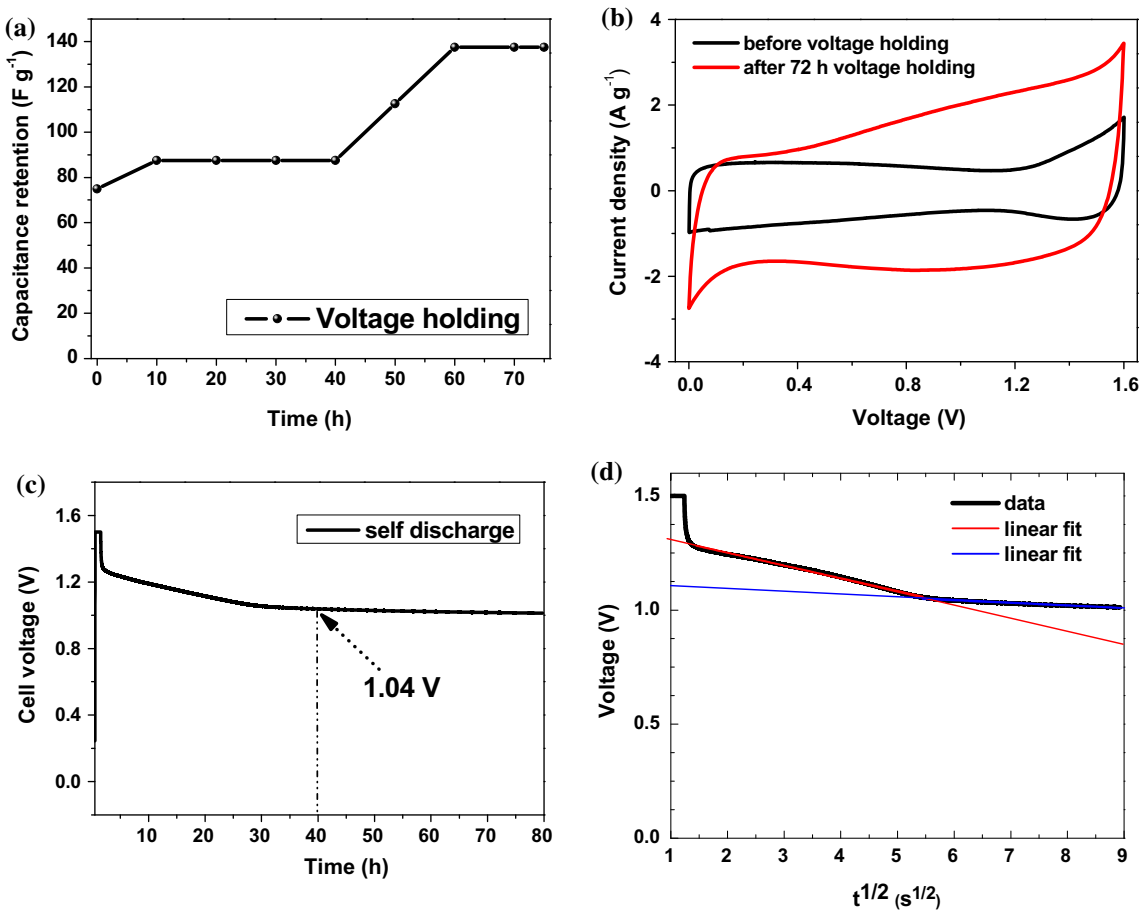

Figure 4 **a** Specific capacitance variation with voltage holding time for a period of 72 + h (3 days), **b** CV profile before and after voltage holding, **c** self-discharge profile for a period of 80 h and **d** fitting of self-discharge curve as a function of $t^{1/2}$ with two lines.

density from 6.7 to 12.2 Wh kg^{-1} at 2 A g^{-1}. This corresponds to an approx. 91% energy increase after ageing tests. Therefore, assuming similar increase for all current densities, one can predict an energy density as high as 23.7 Wh kg^{-1} at 0.5 A g^{-1} and 11.1 Wh kg^{-1} at 10 A g^{-1} after voltage holding.

Note that the energy density at 10 A g^{-1}, after ageing test, is almost equal to that of the cell at 0.5 A g^{-1}, before the ageing test. Thus, a good approach in optimizing the energy density of this symmetric supercapacitor will be to use it after ageing test. This symmetric supercapacitor matches the energy density of supercapacitors reported in the literature and even outperformed them in certain cases as shown Table 2. These excellent electrochemical properties of the symmetric cell are also linked to the small solution and charge transfer resistances observed from Fig. 3e.

In order to elucidate the increase in the specific capacitance value after ageing test, the CV curves before and after floating test are shown in Fig. 4b. A higher charge separation was observed after floating, owing to the augmentation of accessible pores for energy storage after the floating test.

This is in line with the increase in the specific capacitance value since more ions can be stored after floating, substantially increasing the specific capacitance.

Self-discharge experiment, related to the loss of voltage associated with the difference in Gibbs' energy between the charged and the discharged states, was also performed.

The results from tests performed on the cell are as presented in Fig. 4c. The cell was charged up to 1.5 V and held at this potential for 1 h in order to minimize charge redistribution. Thereafter, the behaviour of the cell at open-circuit voltage was investigated.

Since no current can flow through an external circuit in open circuit configuration, only Faradaic reactions dissolving impurities in the electrolyte, decomposition of the electrolyte or more Faradaic reactions occurring at the surface of the electrode material, can explain the self-discharge phenomenon. A steep decrease in the voltage down to 1.27 V within the first minute of self-discharge is noticed.

This was followed by a much slower discharge up to 1.04 V from 40 up to 80 h. The first voltage loss could be associated with the instability of the aqueous electrolyte which could generate oxygen.

This phenomenon becomes more apparent when the applied voltage is removed unlike in previous experiment shown in this study. The instability of the electrolyte becomes less visible below 1.27 V, which coincides with thermodynamic potential of water at 1.23 V.

Diffusion-controlled mechanism for self-discharge can be fitted with Eq. (5) below:

$$V_t = V_i - m \cdot t^{1/2}, \tag{5}$$

Table 2 Comparison of the properties of symmetric cells based on carbonaceous-type materials and PPY in aqueous electrolytes

Symmetric cell	Electrolyte	I (A g^{-1})	v (mV s^{-1})	E_d (Wh kg^{-1})	P_d (W kg^{-1})	References
Activated carbon-fibre with NaOH and KOH	6 M KOH	–	50	8.1	–	[35]
Activated carbon from pomelo peel	1 M $NaNO_3$	0.50	–	17.1	420	[36]
Carbon nanopetal/PPY nanocomposite	1 M LiClO4	–	–	38.9 Wh kg^{-1}	–	[37]
Polypyrrole/carbon fibres	$LiClO_4$/PVA gel electrolyte	–	–	1.0	680	[38]
Reduced graphite oxide	1 M Na_2SO4_4	0.10	–	10.4	–	[39]
3-D carbon framework	1 M Na_2SO4_4	0.20	–	12	400	[40]
Mesoporous carbon	6 M KOH	0.05	–	7.84	–	[41]
Hierarchical porous carbon	KOH/PVA	0.50	–	19.74	500	[42]
N-doped carbon network	1 M Na_2SO_4		–	24.8	29600	[43]
Nanoporous carbon	2.5 M KNO_3	0.50	–	12.4 (BF)[a] 22.7 (AF)[b]	404 (BF)	This work

[a]Before floating test

[b]After floating test

where V_t is the voltage at a given self-discharge time, V_i is the maximum voltage, t is the self-discharge time and m is a constant which depends on the diffusion and geometrical parameters of the material electrode [44].

In other words, the plot of V_t as a function of $t^{1/2}$ must be linear for a diffusion-controlled self-discharge mechanism. As shown in Fig. 4d, the curve can be fitted with two lines with different m-value, suggesting two diffusion-controlled mechanisms. Therefore, one could think of the possible involvement of O_2 and H_2 generated from the electrolyte decomposition. These elements can deplete the ions stored at each interface with the electrode material, forming new species that could dissolve in the electrolyte [45]. A lowering of the initial voltage applied below the thermodynamic potential of water could mitigate this self-discharge phenomenon. However, a relatively good potential of 1.04 V was still maintained on the cell up to 80 h of self-discharge.

Conclusion

In this experiment, the textural properties and electrochemical performance of activated carbon synthesized from a conducting polypyrrole polymer (AC-PPY) was determined. The AC-PPY was prepared using a chemical activation method with varying amounts of K_2CO_3 activating agent to polymer raw materials (AA:PP) in the ratios 0:1, 2:1, 4:1, 6:1 and 8:1.

The samples were then carbonized via a chemical vapour deposition system at 800 °C for a period of 2 h. From the BET results obtained, an optimized 6:1 AA:PP ratio yielded the sample with the highest BET specific surface area and pore volume combination. Further increase in the amount of activating agent only resulted in a decrease in both the SSA and pore volume recorded.

The initial three-electrode electrochemical tests showcased the AC-PPY-6 sample electrode giving the highest current response from the cyclic voltammetry test within an operating potential window of 0.8 V in both positive and negative ranges. The CV curves all exhibited the characteristic EDLC rectangular response signifying the charge storage mechanism were mainly electrostatic in origin. From the chronopotentiometry sample tests, the AC-PPY-6 sample also had the highest discharge time and corresponding specific capacitance (C_S) calculated from the slope of the discharge plot. The C_S values decreased with increasing specific current, which is linked to the failure of ions to adequately access inner charge storage porous sites due to the limited ion transport at increased current densities [46, 47] The electrochemical impedance spectroscopy test correlated with the results obtained from the CD and CV tests with the sample with the AA:PP of 6:1 exhibiting the shortest charge transfer resistance and diffusion length for successful ion transport.

A symmetric device fabricated from the optimized sample recorded an operating voltage of 1.60 V as shown in the cyclic voltammetry tests. The quasi-rectangular shape of the CV curves was maintained, demonstrating the fast ion diffusion kinetics and fast current response on voltage reversal. A specific capacitance of 140 F g^{-1} was obtained at a 0.5 A g^{-1} specific current. The cell retained 99% of its initial capacitance after continuously cycling for 10000 charge–discharge cycles at 2.0 A g^{-1}, showing that there is no significant deterioration (relative stability) of the electrode material assembled in the device. An extended ageing test was conducted to further confirm the device stability at its maximum operating voltage with charge–discharge tests included to monitor the specific capacitance at 10-h intervals. The device specific capacitance was pointedly found to improve after voltage holding tests which was linked to the wettability of the electrode coupled with its ability to store more ions as well as the generation of initially redundant pores which were not participating in the initial storage process. The specific capacitance of the device increased from 75 to 137.5 F g^{-1} at 2.0 A g^{-1} at after the ageing test. This tallied with a similar increase in the device energy density from 6.7 to 12.2 Wh kg^{-1} at a current density of 2.0 A g^{-1} suggesting ageing tests as a potential route to improving device performance.

Acknowledgements

This work is based on the research supported by the South African Research Chairs Initiative of the Department of Science and Technology, Republic of South Africa, and National Research Foundation of South Africa (Grant No. 61056). Any opinion, finding, conclusion or recommendation expressed in this

material is that of the author(s), and the NRF does not accept any liability in this regard. B. S. Moyo will like to acknowledge the SARChI Chair in Carbon for funding her Masters' Degree project. D. Momodu will like to acknowledge financial support from the National Research Foundation (NRF) for his post-doctoral study. Finally, the authors would like to specially thank Dr. Farshad Barzegar of the Electrical and Electronics Engineering Department for his inputs through the invaluable and fruitful discussions which contributed to the final preparation of this work.

Electronic supplementary material: The online version of this article (https://doi.org/10.1007/s10853-017-1911-y) contains supplementary material, which is available to authorized users.

References

[1] Simon P, Gogotsi Y, Dunn B (2014) Where do batteries end and supercapacitors begin? Science 80(343):1210–1211

[2] Lukatskaya MR, Dunn B, Gogotsi Y (2016) Multidimensional materials and device architectures for future hybrid energy storage. Nat Commun 7:12647

[3] Chabi S, Peng C, Hu D, Zhu Y (2014) Ideal three-dimensional electrode structures for electrochemical energy storage. Adv Mater 26:2440–2445

[4] Béguin F, Presser V, Balducci A, Frackowiak E (2014) Carbons and electrolytes for advanced supercapacitors. Adv Mater 26:2219–2251, 2283

[5] Pandolfo AG, Hollenkamp AF (2006) Carbon properties and their role in supercapacitors. J Power Sources 157:11–27

[6] Simon P, Gogotsi Y (2008) Materials for electrochemical capacitors. Nat Mater 7:845–854

[7] Simon P, Gogotsi Y (2013) Capacitive energy storage in nanostructured carbon-electrolyte systems. Acc Chem Res 46:1094–1103

[8] Nishihara H, Kyotani T (2012) Templated nanocarbons for energy storage. Adv Mater 24:4473–4498

[9] Yu C, Fan J, Tian B et al (2002) High-yield synthesis of periodic mesoporous silica rods and their replication to mesoporous carbon rods. Adv Mater 14:1742–1745

[10] Meng W, Chen W, Zhao L, Huang Y, Zhu M, Huang Y, Fu Y, Geng F, Yu J, Chen X, Zhi C (2014) Porous Fe_3O_4/carbon composite electrode material prepared from metal-organic framework template and effect of temperature on its capacitance. Nano Energy 8:133–140

[11] Kyotani T, Ma Z, Tomita A (2003) Template synthesis of novel porous carbons using various types of zeolites. Carbon 41:1451–1459

[12] Basavalingu B, Calderon Moreno JM, Byrappa K et al (2001) Decomposition of silicon carbide in the presence of organic compounds under hydrothermal conditions. Carbon 39:1763–1766

[13] Lillo-Rodenas MA, Cazorla-Amoros D, Linares-Solano A et al (2003) Understanding chemical reactions between carbons and NaOH and KOH: an insight into the chemical activation mechanism. Carbon 41:267–275

[14] Raymundo-Pinero E, Azais P, Cacciaguerra T et al (2005) KOH and NaOH activation mechanisms of multiwalled carbon nanotubes with different structural organisation. Carbon 43:786–795

[15] Wang T, Tan S, Liang C (2009) Preparation and characterization of activated carbon from wood via microwave-induced $ZnCl_2$ activation. Carbon 47:1880–1883

[16] Liu Q-S, Zheng T, Wang P, Guo L (2010) Preparation and characterization of activated carbon from bamboo by microwave-induced phosphoric acid activation. Ind Crops Prod 31:233–238

[17] Wang J, Kaskel S (2012) KOH activation of carbon-based materials for energy storage. J Mater Chem 22:23710

[18] Wei L, Sevilla M, Fuertes AB et al (2011) Hydrothermal carbonization of abundant renewable natural organic chemicals for high-performance supercapacitor electrodes. Adv Energy Mater 1:356–361

[19] Qie L, Chen W, Xu H et al (2013) Synthesis of functionalized 3D hierarchical porous carbon for high-performance supercapacitors. Energy Environ Sci 6:2497

[20] Sevilla M, Mokaya R, Fuertes AB (2011) Ultrahigh surface area polypyrrole-based carbons with superior performance for hydrogen storage. Energy Environ Sci 4:2930–2936

[21] Bello A, Manyala N, Barzegar F, Khaleed AA, Momodu DY, Dangebegnon JK (2016) Renewable pine cone biomass derived carbon materials for supercapacitor application. RSC Adv 6:1800–1809

[22] Momodu D, Madito M, Barzegar F, Bello A, Khaleed AA, Olaniyan O, Dangbegnon J, Manyala N (2016) Activated carbon derived from tree bark biomass with promising material properties for supercapacitors. J Solid State Electrochem 21:859–872

[23] Sevilla M, Fuertes AB (2016) A green approach to high-performance supercapacitor electrodes: the chemical activation of hydrochar with potassium bicarbonate. Chemsuschem 9:1880–1888

[24] Snook GA, Kao P, Best AS (2011) Conducting-polymer-based supercapacitor devices and electrodes. J Power Sources 196:1–12

[25] Huang Y, Li H, Wang Z, Zhu M, Pei Z, Xie Q, Huang Y, Zhi C (2016) Nanostructured polypyrrole as a flexible electrode material of supercapacitor. Nano Energy 22:422–438

[26] Huang Y, Tao J, Meng W, Zhu M, Huang Y, Fu Y, Gao Y, Zhi C (2015) Super-high rate stretchable polypyrrole-based supercapacitors with excellent cycling stability. Nano Energy 11:518–525

[27] Yang P, Mai W (2014) Flexible solid-state electrochemical supercapacitors. Nano Energy 8:274–290

[28] Bello A, Barzegar F, Madito MJ et al (2017) Floating of PPY derived carbon based symmetric supercapacitor in alkaline electrolyte. ECS Trans 6:3–5

[29] Bello A, Barzegar F, Madito MJ, Momodu DY, Khaleed AA, Mashikhwa TM, Dangbegnon JK, Manyala N (2016) Stability studies of polypyrrole-derived carbon based symmetric supercapacitor via potentiostatic floating test. Electrochim Acta 213:107–114

[30] Yao L, Yang G, Han P, Tang Z, Yang J (2016) Three-dimensional beehive-like hierarchical porous polyacrylonitrile-based carbons as a high performance supercapacitor electrodes. J Power Sources 315:209–217

[31] Mao Y, Duan H, Xu B et al (2012) Lithium storage in nitrogen-rich mesoporous carbon materials. Energy Environ Sci 5:7950

[32] Sadezky A, Muckenhuber H, Grothe H, Grothe H, Niesnner R, Poschl U (2005) Raman microspectroscopy of soot and related carbonaceous materials: spectral analysis and structural information. Carbon 43:1731–1742

[33] Zhang H, Zhang L, Chen J, Su H, Liu F, Yang W (2016) One-step synthesis of hierarchically porous carbons for high-performance electric double layer supercapacitors. J Power Sources 315:120–126

[34] Momodu DYY, Barzegar F, Abdulhakeem B, Dangbegnon J, Masikhwa T, Madito M, Manyala N (2015) Simonkolleite-graphene foam composites and their superior electrochemical performance. Electrochim Acta 151:591–598

[35] Hu S, Zhang S, Pan N, Lo Hsieh Y (2014) High energy density supercapacitors from lignin derived submicron activated carbon fibers in aqueous electrolytes. J Power Sources 270:106–112

[36] Peng C, Lang J, Xu S, Wang X (2014) Oxygen-enriched activated carbons from pomelo peel in high energy density supercapacitors. RSC Adv 4:54662–54667

[37] Cherusseri J, Kar KK (2016) Hierarchical carbon nanopetal/polypyrrole nanocomposite electrodes with brush-like architecture for supercapacitors. Phys Chem Chem Phys 18:8587–8597

[38] Chang Y, Han G, Chang Y, Xiao Y, Hou W, Zhou W (2017) Flexible and compressible electrochemical capacitors based on polypyrrole/carbon fibers integrated into sponge. J Alloys Compd 708:1206–1215

[39] Shivakumara S, Kishore B, Penki TR, Munichandraiah N (2014) Symmetric supercapacitor based on partially exfoliated and reduced graphite oxide in neutral aqueous electrolyte. Solid State Commun 199:26–32

[40] Bello A, Barzegar F, Momodu D, Dangbegnon J, Taghizadeh F, Manyala N (2015) Symmetric supercapacitors based on porous 3D interconnected carbon framework. Electrochim Acta 151:386–392

[41] He X, Li R, Qiu J et al (2012) Synthesis of mesoporous carbons for supercapacitors from coal tar pitch by coupling microwave-assisted KOH activation with a MgO template. Carbon 50:4911–4921

[42] Hao P, Zhao Z, Tian J et al (2014) Hierarchical porous carbon aerogel derived from bagasse for high performance supercapacitor electrode. Nanoscale 6:12120–12129

[43] Wang Q, Yan J, Xiao Y et al (2013) Interconnected porous and nitrogen-doped carbon network for supercapacitors with high rate capability and energy density. Electrochim Acta 114:165–172

[44] Andreas HA (2015) Self-discharge in electrochemical capacitors: a perspective article. J Electrochem Soc 162:A5047–A5053

[45] Oickle AM (2013) A systematic study of self-discharge mechanisms in carbon-based, aqueous electrolyte electrochemical capacitors. Ph.D. dissertation, Chemistry Department, Dalhousie University

[46] Reddy RN, Reddy RG (2006) Porous structured vanadium oxide electrode material for electrochemical capacitors. J Power Sources 156:700–704

[47] Lao ZJ, Konstantinov K, Tournaire Y et al (2006) Synthesis of vanadium pentoxide powders with enhanced surface-area for electrochemical capacitors. J Power Sources 162:1451–1454